PHYSICAL REVIEW B, VOLUME 65, 155302

Resonant states induced by impurities in heterostructures

A. Blom,[1] M. A. Odnoblyudov,[1,2] I. N. Yassievich,[1,2] and K. A. Chao[1]
[1]*Division of Solid State Theory, Department of Physics, Lund University, S-223 62 Lund, Sweden*
[2]*A. F. Ioffe Physico-Technical Institute, Russian Academy of Science, 194021 St. Petersburg, Russia*
(Received 23 October 2001; published 18 March 2002)

A study of the formation of resonant states in the conduction band, induced by impurities outside heterostructure quantum wells, is presented. We derive general expressions for the capture and scattering amplitudes, the resonance position and width, and we also calculate the effect on the energy spectrum and the density of states in the quantum well. The theory is applied to two typical impurity potentials, the zero-range potential of deep levels and the Coulomb potential. It is found that the perturbation of the density of states can be significant over wide energy intervals, and that the resonance position may behave nonmonotonically with the modulation-doping distance. The resonance width decays exponentially with the distance, but becomes of the same order as the band discontinuity as we approach close to the quantum well interface. The capture and scattering coefficients may vary by several orders of magnitude over narrow energy intervals, producing a pronounced and strong scattering mechanism.

DOI: 10.1103/PhysRevB.65.155302 PACS number(s): 73.21.Fg, 73.20.Hb

I. INTRODUCTION

Modulation-doped semiconductor heterostructures have been under extensive experimental and theoretical study for the last few decades.[1] In such structures, impurities located in the barrier material supply carriers to the conduction channel, but also act as the source of a long-range scattering potential for these carriers. The effects of elastic scattering in this framework have been studied in numerous works.[2] At the same time, impurity-induced resonant states can be formed, due to the overlap of the localized impurity orbitals with the two-dimensional (2D) continuum states in the conduction channel. In result, alongside elastic scattering of carriers in the conduction channel, the impurities induce strong resonant scattering. Thus, carriers from the 2D continuum states can be captured into localized states, and subsequently be reemitted back. Such generation-recombination processes may lead to new and unexpected features of the shot-noise characteristics[3] of devices based on semiconductor heterostructures.

Coulombic impurities in the valence band have been studied in bulk semiconductors under uniaxial strain.[4] It was found, that the energy spectrum and the density of states can be strongly perturbed due to the formation of resonant states. This in turn will have consequences for optical transitions and kinetic processes.[5,6] The influence of resonant scattering on the current-voltage characteristics of strained bulk p Ge has also been observed.[7]

In this paper we will consider resonant states in the conduction band of heterostructures. These states can be induced by both the Coulomb potential of shallow donors, and an effective short-range potential produced by deep donors, which appear as a result of the doping in the heterostructure barrier region.[8–10] We will derive expressions for the capture and scattering amplitudes, the energy position and width of the resonant state, as well as the density of states of the perturbed spectrum.

The paper is organized in the following way. The general considerations of resonant states based on the theory by Fano[11] and Dirac[12] are presented in Sec. II. In Sec. III this theory is applied to the case of $Al_{0.3}Ga_{0.7}As/GaAs$ heterostructures with deep donor centers, which we treat in the framework of a zero-range potential model. We then proceed to consider donor impurities represented by the Coulomb potential in Sec. IV, and we apply this model to the same system as in Sec. III, still assuming deep donors. Finally we consider a modulation-doped structure with shallow donors, where the charge redistribution in the structure is also taken into account.

II. MODEL DESCRIPTION

In this section we will describe a general treatment of systems that consist of a quantum well (QW) and an impurity located in the barrier region. We denote by $V(z)$ and $V_c(\mathbf{r})$ the potentials of the QW and the isolated impurity, respectively. The total Hamiltonian of such a system has the form

$$\hat{H} = -\frac{\hbar^2}{2m}\nabla^2 + V(z) + V_c(\mathbf{r}), \tag{1}$$

where m is the effective electron mass that may depend on the z coordinate, which is parallel to the QW growth direction. According to Fano,[11] we use different zero-order Hamiltonians to describe the unperturbed localized and 2D quantum well states. Thus, the localized orbital wave function should satisfy the Schrödinger equation

$$\left[-\frac{\hbar^2}{2m}\nabla^2 + V_c(\mathbf{r})\right]\phi(\mathbf{r}) = E_c\phi(\mathbf{r}), \tag{2}$$

and the wave functions of the quantum well states should be found from

$$\left[-\frac{\hbar^2}{2m}\nabla^2 + V(z)\right]\psi_{n\mathbf{k}}(\mathbf{r}) = \mathcal{E}_{n\mathbf{k}}\psi_{n\mathbf{k}}(\mathbf{r}), \tag{3}$$

 ©2002 The American Physical Society

where $\mathbf{k}$ is the wave vector in the QW plane, and n enumerates the space quantization subbands.

The resonant state is a hybridized product of a localized orbital and the 2D continuum states in the QW. We construct the total resonant state wave function $\Psi_{n\mathbf{k}}(\mathbf{r})$ in a typical form for scattering problems, which following Dirac[12] yields (in the following we suppress the coordinate arguments)

$$\Psi_{n\mathbf{k}}=\psi_{n\mathbf{k}}+c_{n\mathbf{k}}\phi+\sum_{n'\mathbf{k}'}\frac{t_{\mathbf{k}\mathbf{k}'}^{nn'}}{E_{n\mathbf{k}}-\mathcal{E}_{n'\mathbf{k}'}+i0}\psi_{n'\mathbf{k}'}. \quad (4)$$

We limit the sum over n' and $\mathbf{k}'$ in Eq. (4) to include only states $\psi_{n'\mathbf{k}'}$ in the energy region close to the resonance. Nevertheless, since both $c_{n\mathbf{k}}$ and $t_{\mathbf{k}\mathbf{k}'}^{nn'}$ decay rapidly (due to the resonant behavior; see below) as we move away from the resonance, we can extend the summation over $\mathbf{k}'$ to infinity and include all bound QW subbands below the resonance.

The resonant state wavefunction should satisfy the Schrödinger equation with the total Hamiltonian (1),

$$\hat{H}\Psi_{n\mathbf{k}}=E_{n\mathbf{k}}\Psi_{n\mathbf{k}}. \quad (5)$$

In Eq. (4), $c_{n\mathbf{k}}$ and $t_{\mathbf{k}\mathbf{k}'}^{nn'}$ are the capture and scattering coefficients, respectively. The influence of a single impurity on the 2D energy spectrum is negligible, and thus for the purpose of calculating these coefficients we may assume $E_{n\mathbf{k}}=\mathcal{E}_{n\mathbf{k}}$.

Substituting Eq. (4) into Eq. (5) and using standard procedures,[12] we find the following expressions:

$$c_{n\mathbf{k}}=\frac{R_{n\mathbf{k}}/\mathcal{L}}{\mathcal{E}_{n\mathbf{k}}-(E_c+\Delta E_{n\mathbf{k}})+i\Gamma_{n\mathbf{k}}/2}, \quad (6)$$

$$t_{\mathbf{k}\mathbf{k}'}^{nn'}=\frac{V_{\mathbf{k}'\mathbf{k}}^{n'n}}{\mathcal{L}^2}+\frac{c_{n\mathbf{k}}}{\mathcal{L}}X_{\mathbf{k}\mathbf{k}'}^{nn'}, \quad (7)$$

where $\mathcal{L}^2$ is the normalization area for the 2D continuous states in the QW, and

$$\Delta E_{n\mathbf{k}}=\Delta-\frac{1}{(2\pi)^2}\sum_{n'}\int d^2\mathbf{k}'\,W_{n'\mathbf{k}'}X_{\mathbf{k}\mathbf{k}'}^{nn'}+\frac{1}{(2\pi)^2}\sum_{n'}\mathrm{P}\int d^2\mathbf{k}'\frac{V_{n'\mathbf{k}'}X_{\mathbf{k}\mathbf{k}'}^{nn'}}{\mathcal{E}_{n\mathbf{k}}-\mathcal{E}_{n'\mathbf{k}'}}, \quad (8)$$

$$\frac{\Gamma_{n\mathbf{k}}}{2}=\frac{\pi}{(2\pi)^2}\sum_{n'}\int d^2\mathbf{k}'\,V_{n'\mathbf{k}'}X_{\mathbf{k}\mathbf{k}'}^{nn'}\delta(\mathcal{E}_{n\mathbf{k}}-\mathcal{E}_{n'\mathbf{k}'}), \quad (9)$$

$$R_{n\mathbf{k}}=V_{n\mathbf{k}}-\frac{1}{(2\pi)^2}\sum_{n'}\int d^2\mathbf{k}'\,V_{\mathbf{k}'\mathbf{k}}^{n'n}W_{n'\mathbf{k}'}. \quad (10)$$

Here P means the Cauchy principal value of an integral, and the following notation for the matrix elements has been introduced:

$$X_{\mathbf{k}\mathbf{k}'}^{nn'}=Z_{n'\mathbf{k}'}^{*}-(\mathcal{E}_{n\mathbf{k}}-E_c)W_{n'\mathbf{k}'}^{*},$$

$$W_{n\mathbf{k}}/\mathcal{L}=\langle\phi|\psi_{n\mathbf{k}}\rangle,$$

$$\Delta=\langle\phi|V(z)|\phi\rangle,$$

$$V_{n\mathbf{k}}/\mathcal{L}=\langle\phi|V_c|\psi_{n\mathbf{k}}\rangle,$$

$$V_{\mathbf{k}\mathbf{k}'}^{nn'}/\mathcal{L}^2=\langle\psi_{n\mathbf{k}}|V_c|\psi_{n'\mathbf{k}'}\rangle,$$

$$Z_{n\mathbf{k}}/\mathcal{L}=\langle\phi|V(z)|\psi_{n\mathbf{k}}\rangle. \quad (11)$$

In the expressions (6) and (7) we have neglected terms that are of the second order in the impurity potential V_c. This corresponds to the Born approximation in conventional scattering theory.[13]

One can see from Eq. (6) that the capture amplitude $|c_{n\mathbf{k}}|^2$, which gives the contribution of the localized state to the hybridized one, exhibits a resonance behavior, shifted from the energy of the localized state E_c by $\Delta E_{n\mathbf{k}}$. The value of the shift $\Delta E_{n\mathbf{k}}$, the width $\Gamma_{n\mathbf{k}}$ and the numerator $R_{n\mathbf{k}}$ all depend on the energy itself, as indicated by the index $\mathbf{k}$. We, therefore, define the resonance energy as the energy at which $|c_{n\mathbf{k}}|^2$ acquires its maximum. The lifetime $\tau_r=\hbar/\Gamma_{n\mathbf{k}}$ of the resonant state can then be found to a good approximation by evaluating $\Gamma_{n\mathbf{k}}$ at this energy.

The hybridization of the continuous states with the localized orbital will also perturb the energy spectrum and modify the density of states in the QW. To calculate this we use the identity

$$\langle\Psi_{n\mathbf{k}}|\hat{H}|\Psi_{n\mathbf{k}}\rangle=E_{n\mathbf{k}}\langle\Psi_{n\mathbf{k}}|\Psi_{n\mathbf{k}}\rangle. \quad (12)$$

As noted above, a single impurity has a negligible influence on the energy $E_{n\mathbf{k}}$ and the total wave function $\Psi_{n\mathbf{k}}$, which is reflected in the appearance of the factors $\mathcal{L}$ in Eqs. (6) and (7). More specifically, the influence on the energy will be $E_{n\mathbf{k}}=\mathcal{E}_{n\mathbf{k}}+\mathcal{O}(1/\mathcal{L}^2)$, and the total wave function will be normalized to within a similar factor; $\langle\Psi_{n\mathbf{k}}|\Psi_{n\mathbf{k}}\rangle=1+\mathcal{O}(1/\mathcal{L}^2)$.

If instead there is a finite number N_d of impurities, we must take into account the contribution from each. Assuming a low enough doping concentration, such that the overlaps of the impurity wave functions at different sites are negligible, the impurities can be considered as noninteracting. In this case, their total effect is given by multiplying the influence of a single impurity by the number of donors. By evaluating the left- and right-hand sides of Eq. (12) separately, and summing over all impurities, we then arrive at

$$E_{n\mathbf{k}}=\mathcal{E}_{n\mathbf{k}}+n_{2\mathrm{D}}\left[\tilde{E}\frac{R_{n\mathbf{k}}^2-2V_{n\mathbf{k}}R_{n\mathbf{k}}}{\tilde{E}^2+\Gamma_{n\mathbf{k}}^2/4}-V_{\mathbf{k}\mathbf{k}}^{nn}\right], \quad (13)$$

where $\tilde{E}\equiv E_{n\mathbf{k}}-(E_c+\Delta E_{n\mathbf{k}})$ and $n_{2\mathrm{D}}\equiv N_d/\mathcal{L}^2$ is the sheet density of donors. This is an equation for $E_{n\mathbf{k}}$ that should be solved to establish the relationship between the perturbed spectrum $E_{n\mathbf{k}}$ and the corresponding wave-function label $\mathbf{k}$.

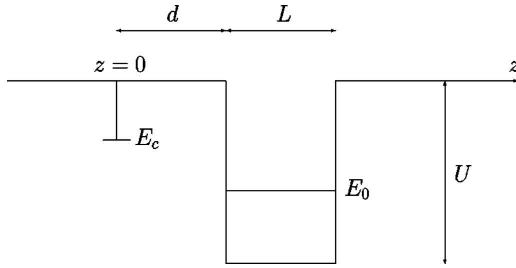

FIG. 1. Schematic picture of the square quantum well structure used for the deep donor centers in both the zero-range potential approximation of Sec. III and for the Coulomb potential in Sec. IV B.

Given the energy spectrum, we may proceed to calculate the density of states per spin in each subband. Assuming that the conduction-band spectrum is isotropic, this is given by

$$\rho_n(E_{nk}) = \frac{1}{2\pi}\frac{k(E_{nk})}{\partial E_{nk}/\partial k}. \tag{14}$$

For isolated impurities the density of states is a δ function, whereas for the pure 2D quantum well states it is constant. The formation of the resonant state due to the hybridization of the band states with the localized donor state will lead to a density of states that exhibits a combination of these two features. This has been shown to have important consequences for, e.g., optical properties.[4]

By its definition in Eq. (4), the coefficient $c_{n\mathbf{k}}$ is directly related to the probability for capture into the localized part of the resonant state.[4–6] This process will give a nontrivial contribution to the electron distribution function, which in turn will affect the current and the current noise in the QW.

III. ZERO-RANGE POTENTIAL APPROXIMATION

In this section we will apply the above described general approach to study resonant states induced by a short-range impurity potential. The calculations will be performed for the case of deep donor centers that appear in the barrier region of $Al_{0.3}Ga_{0.7}As/GaAs/Al_{0.3}Ga_{0.7}As$ heterostructures (Fig. 1) doped by Si. These centers were extensively studied experimentally[8–10] because they strongly affect the performance of heterostructure based electronic and optoelectronic devices.

It was shown[8] that in doped $Al_xGa_{1-x}As$ with Al content x larger than 0.27, more than half of the Si donor centers produce deep levels with binding energy $\simeq 155$ meV measured from the bottom of the Γ valley. The fraction of deep donors increases with increasing Al mole fraction.

We will describe these localized deep states in the framework of a zero-range potential model.[13] This approach assumes that the localized state wave function $\phi(\mathbf{r})$ should be a solution of the Schrödinger equation

$$\left[-\frac{\hbar^2}{2m_b}\nabla^2 + V_c(\mathbf{r})\right]\phi(\mathbf{r}) = E_c\phi(\mathbf{r}), \tag{15}$$

where the spherically symmetric impurity potential $V_c(\mathbf{r})$ has a finite nonzero value only within distances comparable to the lattice constant, near the impurity. The wave function of the localized state should satisfy the boundary condition

$$\frac{1}{(r\phi)}\frac{\partial(r\phi)}{\partial r}\Big|_{r\to 0} = -\kappa, \tag{16}$$

where κ is related to the energy of the localized state by

$$E_c = -\frac{\hbar^2\kappa^2}{2m_b}, \tag{17}$$

and can be considered as a characteristic parameter of the potential. The normalized wave function of the isolated localized impurity state that satisfies the boundary condition (16) has the form

$$\phi(\mathbf{r}) = \sqrt{\frac{\kappa}{2\pi}}\frac{e^{-\kappa r}}{r}. \tag{18}$$

The wave functions of the states in the isolated square quantum well for the case of different effective masses m_w and m_b in the well and barrier regions, respectively, are

$$\psi_{n\mathbf{k}}(\mathbf{r}) = \frac{1}{\mathcal{L}}e^{i\mathbf{k}\cdot\boldsymbol{\rho}}\varphi_n(z), \tag{19}$$

where the envelope functions $\varphi_n(z)$ are well known.[13] For an isotropic conduction band, the energy spectrum in the nth subband is given by

$$\mathcal{E}_{n\mathbf{k}} = E_n + \frac{\hbar^2k^2}{2m_w}, \tag{20}$$

and hence we can substitute the wave-vector indices $\mathbf{k}$ by the wave number k.

We consider the case when the localized state is resonant only with the continuum states in the lowest space quantization subband, and skip the index n. To obtain the expressions for ΔE_k and Γ_k in Eqs. (8) and (9), one needs to calculate the matrix element V_k of the impurity potential V_c between the localized state $\phi(\mathbf{r})$ and the quantum well state $\psi_k(\mathbf{r})$. To calculate this matrix element with a general but unspecified short-range impurity potential we use Eq. (2) to express V_k in the form

$$V_k^*/\mathcal{L} \equiv \langle\psi_k|V_c|\phi\rangle = \left\langle \psi_k \left| \frac{\hbar^2}{2m_b}\nabla^2 + E_c \right| \phi \right\rangle. \tag{21}$$

The matrix element of the kinetic energy between the localized state and the QW state wave functions diverges due to the singular behavior of $\phi(\mathbf{r})$ at the impurity position. The details of the calculation of this matrix element are presented in the Appendix.

Following the procedure described in Sec. II, we calculate the resonance position and width as a function of the distance between the impurity and the quantum well for the case of deep Si donors with $E_c = -155$ meV, and for different QW widths. We have used the value $U = 232$ meV for the band offset between the Γ points in the conduction bands

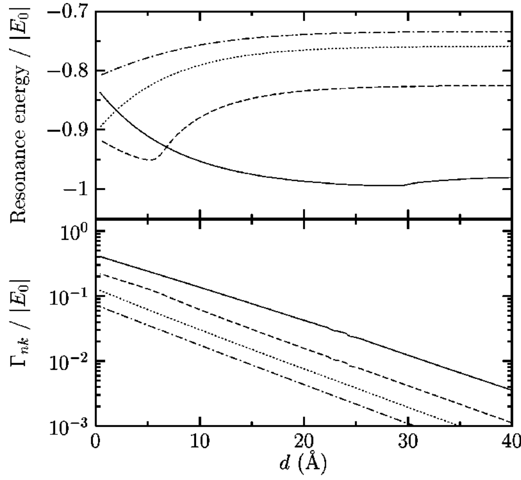

FIG. 2. The resonance energy (upper panel) and the resonant width (lower panel) normalized by the energies of the first space quantization level as a function of the distance d between impurity and QW for the case of deep donor in an $Al_{0.3}Ga_{0.7}As/GaAs/Al_{0.3}Ga_{0.7}As$ heterostructure. $L=50$ Å, $E_0=-157.7$ meV (——); $L=75$ Å, $E_0=-185.6$ meV (– – –); $L=100$ Å, $E_0=-201.8$ meV (· · · ·); $L=125$ Å, $E_0=-208.8$ meV (—·—·).

of GaAs and $Al_{0.3}Ga_{0.7}As$, and for the effective masses in the QW and the barrier region the values 0.067 and 0.092, respectively.

The results of the calculations are presented in Fig. 2. In the upper panel we plot the resonance energy, defined as the position of the maximum of the capture amplitude $|c_k|^2$, for four different well widths. In the lower panel is shown the width of the resonant state, defined as Γ_k evaluated at this resonance energy. A more detailed discussion of these results, along with corresponding ones for the Coulomb potential case, will be given in Sec. IV B.

We observe that for the case of a short-range impurity potential the dependence of the resonant position on the distance between the impurity and the QW can be nonmonotonic when the binding energy of the localized impurity state is close to the position of the space quantization level. The position of the resonance is shifted towards the space quantization level from E_c when the distance decreases, but it does not cross the bottom of the 2D subband. As a result of the interaction between the localized and the 2D states, the resonant level is pushed back from the quantization level at some critical distance.

IV. COULOMB POTENTIAL IMPURITY

A. General considerations

In the simplest case, donors or acceptors in semiconductors are represented by the Coulomb potential

$$V_c(\mathbf{r})=-\frac{e^2}{\epsilon r}. \tag{22}$$

The energy of such a hydrogenic impurity state can be expressed through the effective mass m^* and the dielectric constant ϵ of the host material. The normalized ground-state wave function, which satisfies Eq. (2), is

$$\phi(\mathbf{r})=\frac{1}{\sqrt{\pi a_c^3}}e^{-r/a_c}, \tag{23}$$

where the parameter a_c can be related to the ground-state energy E_c by the expression

$$E_c=-\frac{\hbar^2}{2m^*a_c^2}. \tag{24}$$

For the pure hydrogenic case, a_c coincides with the effective Bohr radius $a_B=\epsilon\hbar^2/m^*e^2$. However, experimentally the binding energy is found to depend also on the particular impurity species. To account for this, an additional phenomenological part is introduced in the impurity potential, the so-called central-cell correction.[14] This correction is assumed to alter the potential in a substantial way only in a region very close to the impurity position, whereas the long-range behavior is still determined by the original Coulomb potential.

In the systems we aim to study in this work, the important processes take place in the quantum well, which is situated at some distance from the impurity. It is, therefore, reasonable to assume, that the matrix elements required to calculate the capture and scattering coefficients, can be evaluated using the Coulomb potential (22) for V_c instead of the true impurity potential.

Moreover, due to the central-cell correction, the impurity wave function should decay faster than the effective Bohr radius. This is especially true if we attempt to treat the type of deep impurities considered in the preceding section with a Coulombic impurity potential. We will, therefore, assume that the impurity binding energy E_c is given, e.g., from experiments, and from it define, using Eq. (24), the localization radius a_c that determines the decay of the wave function (23). We will thus have two characteristic length scales, the radius a_c of the localized state, and the effective Bohr radius a_B that controls the range of the Coulomb potential. This approach will enable us to describe both traditional shallow donors, as well as deeper ones of the type discussed in Sec. III, by the Coulomb potential.

Using the impurity potential (22) and the wave function (23), we can now derive expressions for the matrix elements (11) defined in Sec. II. We will further assume that the difference in dielectric constant between the well and the barrier is negligible, and do not take into account image charges. The conduction band is taken to be isotropic; hence all matrix elements, except $V_{\mathbf{k}'\mathbf{k}}^{n'n}$, can be labeled by the wave number k instead of the wave vector $\mathbf{k}$.

After employing a number of standard integrals, we arrive at the following expressions:

$$\Delta=\frac{1}{a_c}\int_{-\infty}^{\infty}V(z)\left(\frac{|z|}{a_c}+\frac{1}{2}\right)e^{-2|z|/a_c}\,dz,$$

$$Z_{nk}=\frac{2\sqrt{a_c\pi}}{\xi^2}\int_{-\infty}^{\infty}\varphi_n(z)e^{-|z|\xi/a_c}\left(\frac{|z|}{a_c}+\frac{1}{\xi}\right)V(z)dz,$$

$$W_{nk}=\frac{2\sqrt{a_c\pi}}{\xi^2}\int_{-\infty}^{\infty}\varphi_n(z)e^{-|z|\xi/a_c}\left(\frac{|z|}{a_c}+\frac{1}{\xi}\right)dz,$$

$$V_{nk}=\frac{-2\sqrt{\pi}e^2}{\xi\sqrt{a_c}\epsilon}\int_{-\infty}^{\infty}\varphi_n(z)e^{-|z|\xi/a_c}dz, \tag{25}$$

where we have defined $\xi\equiv\sqrt{1+(ka_c)^2}$. The matrix elements decay exponentially with the distance d, since the origin $z=0$ is taken at the impurity position, whereas the wave functions $\varphi_n(z)$ and the potential $V(z)$ are centered around the quantum well.

To calculate the capture and scattering coefficients (6) and (7) we also need to evaluate the matrix element $V^{n'n}_{\mathbf{k}'\mathbf{k}}$, which with the potential (22) becomes

$$V^{n'n}_{\mathbf{k}'\mathbf{k}}=\frac{-2\pi e^2}{\epsilon q}\int_{-\infty}^{\infty}\varphi_n(z)\varphi^*_{n'}(z)e^{-|z|q}dz, \tag{26}$$

where $q\equiv\sqrt{k^2+k'^2-2kk'\cos\theta}$ is the magnitude of the transferred momentum (θ is the angle between $\mathbf{k}$ and $\mathbf{k}'$).

The expression (26), and hence the numerator R_{nk} of the capture coefficient (6) as well as the term $V^{nn}_{\mathbf{kk}}$ in Eq. (13), diverges as $q\rightarrow 0$, corresponding to forward elastic scattering. This is a manifestation of the characteristic long-range nature of the Coulomb potential (22). The singularity is removed by introducing screening by the 2D electron gas (EG) in the quantum well,[15] which can be accounted for by replacing $q\rightarrow q+q_s$ in Eq. (26). The screening constant q_s can be taken as

$$q_s=2\pi\frac{e^2}{\epsilon}D(E_{\mathrm{f}}), \tag{27}$$

where $D(E_{\mathrm{f}})$ is the density of states at the Fermi level, for which we can use the standard expression $m_w/\pi\hbar^2$ if we assume that only the lowest subband is occupied.

The term $V^{nn}_{\mathbf{kk}}$ appearing in Eq. (13) has an unexpected consequence for the perturbed spectrum, as it is in fact independent of $\mathbf{k}$, which can be seen from Eq. (26). Thus also far from the resonance, the bracket in Eq. (13) does not vanish. The reason is that we have treated the problem in the Born approximation, which is valid under the condition that the kinetic energy of the incoming particle is much larger than the strength of the impurity potential. This assumption fails in the limit $k\rightarrow 0$, and thus our results are not strictly applicable there. In the opposite limit $k\rightarrow\infty$ the bracket becomes negligible since $\mathcal{E}_{n\mathbf{k}}\rightarrow\infty$.

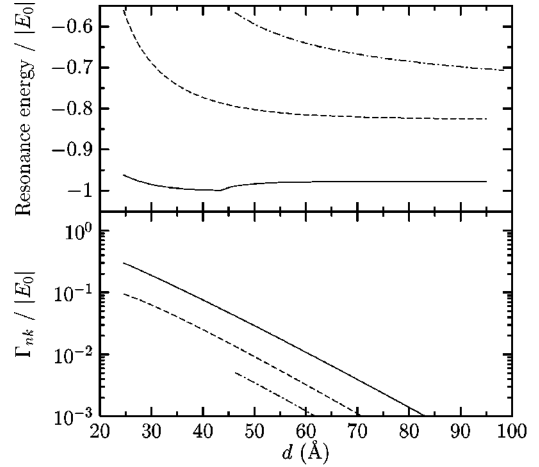

FIG. 3. Position and width of the resonant state for the lowest QW subband as function of the distance d of the impurity from the AlGaAs/GaAs QW. The curves correspond to different well widths: $L=50$ Å (——), $L=75$ Å (– – –), and $L=100$ Å (—·—·). All curves are normalized by the position E_0 of the bottom of the quantization subband (see Fig. 2 for values). In this figure we consider a deep donor, $E_c=-155$ meV.

B. Deep level Coulomb impurity

We now apply the Coulomb potential theory to the same system considered in Sec. III, a deep donor state outside a $Al_{0.3}Ga_{0.7}As/GaAs/Al_{0.3}Ga_{0.7}As$ quantum well (Fig. 1). We use the same quantum well wave functions (19) and the same impurity binding energy, i.e., $E_c=-155$ eV, corresponding to a localization radius $a_c=16.4$ Å, whereas the Bohr radius $a_{\mathrm{B}}=70.2$ Å. The screening length defined by Eq. (27) of the 2DEG in the GaAs layer is $1/q_s=48.2$ Å. Furthermore the isotropic dispersion relation (20) is retained.

In the upper panel of Fig. 3 we plot the calculated resonance energy, which in this case is taken as the position of the maximum of $|c_{nk}|^2$ for the lowest QW subband. The width Γ_{nk} of the resonant state, defined as before in Sec. III, is shown in the lower panel.

Although many features of Figs. 2 and 3 are similar, we note that the horizontal range is quite different; as expected, the long-range Coulomb potential is felt at much larger distances. The resonance position converges towards the unperturbed value E_c as $d\rightarrow\infty$. For the Coulomb potential impurity, the general trend appears to be that the resonance position is pushed up towards the continuum with decreasing distance, in contrast to what we observed for the zero-range potential, where it was instead pulled down towards the bottom of the well. An exception can, however, be found when the impurity level E_c is very close to the bottom of the subband ($L=50$ Å); we then observe a nonmonotonic behavior, for both types of impurity potentials. The resonance cannot cross the quantization level.

In the upper panel of Fig. 4 we plot $|c_{nk}|^2$, again for the lowest subband. We clearly see the Lorentzian shape and the widening of the resonance with decreasing distance d. At large distances the resonance peak becomes very well defined and narrow (exponential decay, as seen in Fig. 3), while the peak height grows exponentially. Thus $|c_{nk}|^2$ behaves as

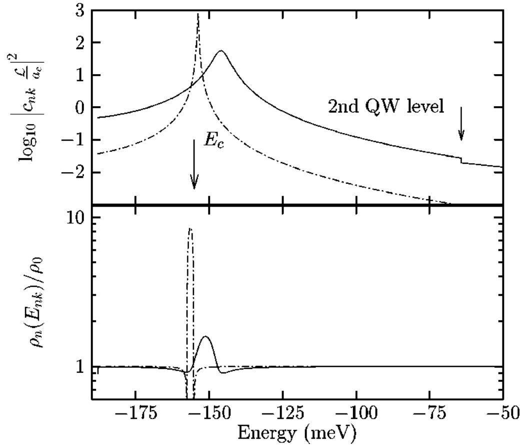

FIG. 4. The capture coefficient $|c_{nk}|^2$ (upper panel) and the density of states (lower panel) for the lowest subband as functions of the energy, for the case $L=75$ Å for the AlGaAs/GaAs QW. The density of states is normalized by the density of states for the unperturbed 2D spectrum $\rho_0=m_w/2\pi\hbar^2$. The doping concentration is taken as 5×10^{11} cm^{-2}, which is consistent with the requirement for noninteracting impurities. The curves correspond to $d/a_c=2.5$ (——) and $d/a_c=4.0$ (— · — ·). The second QW level appears at $E_1=-64.1$ meV.

a δ function as $d\rightarrow\infty$, which is to be expected, since the impurity becomes more or less isolated and does not interact with the well states.

A striking feature of the Coulomb potential case is that, unlike for the zero-range potential, when we approach close to the well, the resonance vanishes. From the lower panel of Fig. 3 we see that in this region the width of the resonant state is comparable to the depth of the quantum well. The capture amplitude becomes essentially independent of the energy, hence no well-defined resonance peak can be found. Instead, the effect of the impurity potential is spread out through the entire spectrum. At the same time, the capture amplitude increases in the energy region close to the QW level, and thus even electrons close to the bottom of the subband can be strongly affected. We should, however, be careful in this interpretation, since our entire approach is based on the existence of a well-defined resonance, which is not shifted too far from its unperturbed value. Thus, in the region close to the QW, the applicability of our method is questionable.

The perturbed density of states $\rho_n(E_{nk})$, defined by Eq. (14) and normalized by the density of states for the unperturbed 2D spectrum, is shown in the lower panel of Fig. 4. It is clear that we have contributions from both the 2D states (constant density of states far from the resonance) and the δ-function-like behavior of an isolated impurity. The region over which the spectrum is perturbed is notable even for $d/a_c=4$, in which case the increase in the density of states is by an order of magnitude at the resonance. The width of the peak in $\rho_n(E_{nk})$ increases with smaller distance d, in complete correspondence with the spreading of the capture amplitude as discussed above, and the peak height decreases accordingly. The density-of-states peak width also depends strongly on the doping concentration, which is not the case for the capture amplitude.

We observe an almost complete depletion of the density of states in the wings of the resonance, just before the sharp increase. This resembles a miniature band gap, which could be possible to observe in optical-absorption measurements.

A further detail seen from Fig. 4 is that the maximum of the capture amplitude does not coincide exactly with the peak in the density of states. The reason can be found in the expression (13) for $E_{n\mathbf{k}}$, where two terms containing $V_{\mathbf{kk}}^{nn}$ (corresponding to direct Coulomb scattering) and $V_{n\mathbf{k}}$ (the interaction of the localized state with the QW state via the Coulomb potential) appear. Without these, the square bracket in Eq. (13) would simply be proportional to $|c_{n\mathbf{k}}|^2$, but in their presence we obtain a so-defined Coulomb shift of the resonance.

A final noteworthy detail in the upper panel of Fig. 4 is the sudden drop in the capture amplitude as we cross the next quantum level. As the subband energy $\mathcal{E}_{n\mathbf{k}}$ crosses a higher level, a further term is introduced in the sum (9) for $\Gamma_{n\mathbf{k}}/2$, and thus the denominator in $|c_{n\mathbf{k}}|^2$ increases abruptly. This corresponds to the increased density of final states available in the second subband. There is no such corresponding step-like behavior in $R_{n\mathbf{k}}$, and thus we will observe a sharp drop in the capture amplitude at each QW level. The discontinuity is most pronounced at small distances and vanishes as $d\rightarrow\infty$.

These discontinuities in the capture amplitude is the reason why for the widest well considered in Fig. 3 ($L=100$ Å), the curve is cut off already at $d/a_c\simeq2.9$. At this distance, the resonance is just about to cross the second QW level, which appears at $E_1=-114.34$ meV. The resonance is in fact carried over from $|c_{0k}|^2$ (used for the definition of the resonance position) into the capture amplitude $|c_{1k}|^2$ (which is defined only for energies $>E_1$) for the next subband, but with much lower amplitude.

If such a discontinuity were to appear in the same energy region as the resonance energy, the resonance peak, both in the capture coefficient and the density of states, would be abruptly cut off. It could, therefore, be possible to control and limit the influence of the resonance scattering by shifting the QW energy levels, either by adjusting the well width or by tuning the doping concentration and thereby the spacer potential barrier height (see Sec. IV C).

C. Shallow Coulomb impurity

A Coulomb potential is more commonly associated with shallow donors. In $Al_{0.3}Ga_{0.7}As$ the impurity binding energy is about 9 meV, while the band discontinuity in the conduction band is 232 meV. To reach the resonance energy, the electrons in a flat quantum well (usually only the lowest few subbands are assumed to be populated) would have to be accelerated to very large energies, and most likely instead be scattered by phonons or other scattering processes.[16,17]

With modulation doping, which is a dominating choice for device applications based on heterostructures,[1] the QW levels can be brought closer to the impurity level. The charge transfer from the doping region, over the undoped spacer

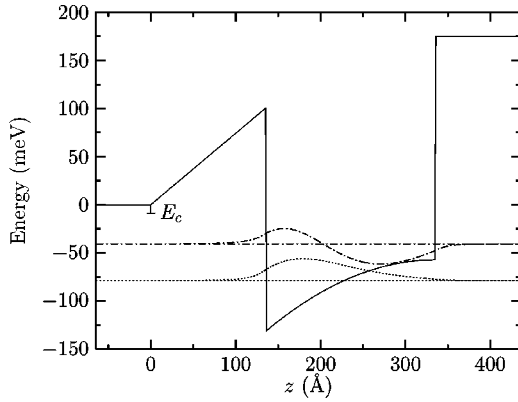

FIG. 5. The modulation-doping profile used for the calculations with shallow donors. For this example is used a well width of $L = 200$ Å and $d/a_c = 2$. The lowest quantization levels (-78.6 meV and -40.6 meV) and their corresponding wave functions $\varphi_n(z)$ are indicated; these are the only levels below E_c.

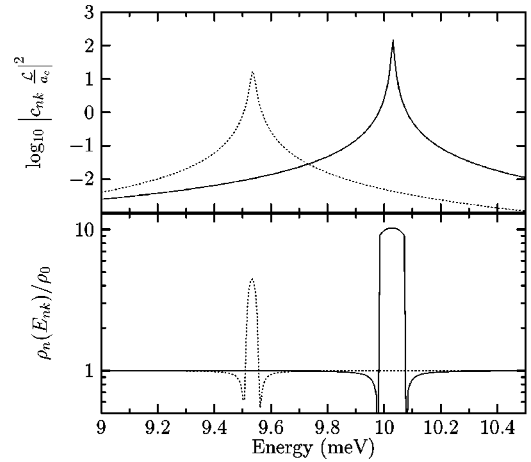

FIG. 6. Results similar to those presented in Fig. 4, but for the modulation-doping potential shown in Fig. 5. The two curves are for $d/a_c = 2.0$ (——) and $d/a_c = 2.5$ (· · · ·).

region $0 < z < d$ into the QW, leads to the buildup of an electric field and a resulting band profile that qualitatively looks like that in Fig. 5.

Still, the distance between the lowest QW levels and the resonant state is rather large, and for low-field mobility measurements the effects of resonant scattering are probably difficult to observe. However, for device operation under high-field conditions, resonant scattering can be an important mechanism.[7] Most scattering processes take place at any energy, with a probability that depends smoothly on the electron momentum.[16,17] In contrast, the resonant scattering as presented here takes place in a very narrow energy range, at least as long as we have a well-defined resonance peak in the capture amplitude. Over this interval the capture and scattering probabilities vary by several orders of magnitude, and thus introduces strong scattering of carriers that have possibility to reach this energy region.

Using a modulation-doped structure with a 2D δ-doping layer at $z = 0$, as shown in Fig. 5 for a particular choice of the distance d, we perform similar calculations as for the deep donor case in the preceding section. For simplicity we consider the charge distribution in the QW to be constant and assume that all donors are ionized. The potential profile is self-consistent in the sense that we confirm that the resulting Fermi level is well below E_c.

The effective localization radius is substantially larger for a shallow donor; in the case under investigation with $E_c = -9$ meV, $a_c = 67.8$ Å, which essentially is equal to the Bohr radius. We continue to use a doping concentration of 5×10^{11} cm^{-2}.

The results for a shallow donor (Fig. 6) are qualitatively similar to those of the preceding section. The resonant level is pushed upward towards the continuum, in this case above zero, but it is still bound. The resonance is also much sharper than before. This is due to the fact that the energy distance is larger between the resonance and the QW level, and thus the quantity ξ that appears in the matrix elements (25) is larger in the resonance region, causing a more rapid decay of the capture coefficient.

V. CONCLUSIONS

We have studied the formation of resonant states in the conduction band of heterostructures, induced by donor impurities situated in the barrier region. Two types of impurity potentials, a short-range potential associated with deep levels and the Coulomb potential, were considered.

The resonant state is a hybridized product of the 2D band states in the quantum well and the localized impurity orbital. As a result, in addition to being elastically scattered off the impurity potential, carriers in the QW subbands also have the possibility to be captured into the localized state, and subsequently be reemitted. This will have several consequences for electrical and optical properties of devices based on modulation-doped heterostructures.

The capture probability is found to exhibit a resonance behavior, with a maximum at an energy shifted from the original impurity energy. The shift may behave nonmonotonically as a function of the doping distance, and is pushed in different directions for the two choices of impurity potentials. The width of the resonance decays exponentially with the doping distance, but becomes comparable to the band offset or the quantum well depth at small distances. The effect of the resonant state is then felt throughout the energy spectrum, also at the bottom of the subband.

For optimal device performance, it is desirable to have a high concentration of carriers in the QW. Thus the modulation-doping layer cannot be placed too far from the heterojunction. On the other hand, if it is placed close to the QW interface, the increased scattering—both resonant and elastic—will deteriorate the current and lower the performance. Thus some optimal distance has to be found by considering all relevant processes involved.

Optical properties are determined by the density of states, which is shown to acquire contributions both from the constant 2D part and the δ-function-like impurity part. The density of states also exhibits a resonance behavior, although the peak need not coincide exactly with the resonance position of the capture probability. A small band gap was observed close to the resonance, and at the resonance, which can be

very wide, the density of states may be enhanced by orders of magnitude.

The electron distribution function and thus the high-field kinetic processes in the QW will be influenced by the strong resonant scattering that takes place in a narrow interval at the resonance energy. We can also expect a pronounced effect on the shot-noise spectrum, due to the carrier capture and re-emission process accompanying the resonant scattering.

ACKNOWLEDGMENTS

This work was performed within the Nanometer Consortium at Lund University, and was supported by grants of the Swedish Foundation for Strategic Research, the Swedish Research Council (Grant No. TFR-THZ 2000-403), NorFA (Grant No. 000384), the Russian Foundation for Basic Research, the Russian Academy of Science, and the Russian Ministry of Science.

APPENDIX

We will use in our derivation that the localized state wave function $\phi(\mathbf{r})$ satisfies the following relation:

$$\frac{\partial \phi}{\partial r} = -\kappa\phi - \frac{\phi}{r}. \tag{A1}$$

First consider the matrix element of the Laplace operator between the states $\phi(\mathbf{r})$ and $\psi_k(\mathbf{r})$.

$$\begin{aligned}\langle \psi_k|\nabla^2|\phi\rangle &= \int d^3\mathbf{r}[\nabla(\psi_k^*\nabla\phi) - \nabla\psi_k^*\nabla\phi]\\ &= \int d^3\mathbf{r}\,\mathrm{div}(\psi_k^*\nabla\phi) - \int d^3\mathbf{r}\,\nabla\psi_k^*\nabla\phi.\end{aligned} \tag{A2}$$

Let us consider the first integral. We surround the origin of the coordinate where the impurity is located by two spheres with radii R_0 and R_1. We will let R_1 tend to infinity and R_0 to zero at the end of the calculation. We now transform the volume integrals to two surface ones using Gauss theorem;

$$\begin{aligned}\int d^3\mathbf{r}\,\mathrm{div}(\psi_k^*\nabla\phi) &= \int_{S_{R_1}} (\psi_k^*\nabla\phi, \mathbf{n}_{R_1}) dS_{R_1}\\ &\quad - \int_{S_{R_0}} (\psi_k^*\nabla\phi, \mathbf{n}_{R_0}) dS_{R_0}\\ &= -\int_{S_{R_0}} (\psi_k^*\nabla\phi, \mathbf{n}_{R_0}) dS_{R_0}.\end{aligned} \tag{A3}$$

The integral over the sphere with radius $R_1 \to \infty$ tends to zero, while the second integral should be considered more carefully,

$$\begin{aligned}\int d^3\mathbf{r}\,\mathrm{div}(\psi_k^*\nabla\phi) &= -\psi_k^*(0)\int_{S_{R_0}} (\nabla\phi, \mathbf{n}_{R_0}) dS_{R_0}\\ &= -\psi_k^*(0)\int_{S_{R_0}} \frac{\partial\phi}{\partial r} dS_{R_0}\\ &= -\psi_k^*(0)\lim_{R_0\to 0} 4\pi R_0^2\\ &\quad \times\left(-\kappa\phi(R_0) - \frac{\phi(R_0)}{R_0}\right)\\ &= 4\pi\psi_k^*(0)\sqrt{\frac{\kappa}{2\pi}}.\end{aligned} \tag{A4}$$

Here we have used that $\psi_k(\mathbf{r})$ varies slowly in the region infinitesimally close to the impurity. This allows us to take it out of the integral with its value at the impurity position. Using the similar procedure one can show that the second integral in Eq. (A2) becomes

$$\int d^3\mathbf{r}\,\nabla\psi_k^*\nabla\phi = -\int d^3\mathbf{r}\,\nabla^2\psi_k^*\phi. \tag{A5}$$

Thus the original matrix element in Eq. (A2) becomes

$$\langle\psi_k|\nabla^2|\phi\rangle = 4\pi\psi_k^*(0)\sqrt{\frac{\kappa}{2\pi}} + \langle\phi|\nabla^2|\psi_k\rangle^\dagger, \tag{A6}$$

where $\langle\cdots\rangle^\dagger$ denotes Hermitian conjugate.

Now we use Eq. (3) to obtain the final expression for the matrix element (21);

$$\begin{aligned}\langle\psi_k|V_c|\phi\rangle &= \langle\psi_k|\phi\rangle E_c + 4\pi\sqrt{\frac{\kappa}{2\pi}}\psi_k^*(0)\frac{\hbar^2}{2m_b}\\ &\quad + \left\langle \psi_k V(z)\left|\frac{m(z)}{m_b}\right|\phi\right\rangle - E_k\left\langle\psi_k\left|\frac{m(z)}{m_b}\right|\phi\right\rangle.\end{aligned} \tag{A7}$$

Thus we have expressed the matrix element with the unknown impurity potential via another matrix elements in Eq. (11).

[1] C. Weisbuch and B. Vinter, *Quantum Semiconductor Structures: Fundamental and Applications* (Academic Press, Boston, 1991), p. 252.
[2] T. Ando, J. Phys. Soc. Jpn. **51**, 3900 (1982).
[3] Ya. M. Blanter and M. Büttiker, *Shot Noise in Mesoscopic Conductors*, Physics Reports Vol. 336 (Elsevier, Amsterdam, 2000).
[4] M.A. Odnoblyudov, I.N. Yassievich, V.M. Chistyakov, and K.A. Chao, Phys. Rev. B **62**, 2486 (2000).
[5] M.A. Odnoblyudov, I.N. Yassievich, M.S. Kagan, Yu.M. Galperin, and K.A. Chao, Phys. Rev. Lett. **83**, 644 (1999).
[6] A.A. Prokof'ev, M.A. Odnoblyudov, and I.N. Yassievich, Semiconductors **35**, 565 (2001).

[7] A.T. Dalakyan, V.N. Tulupenko, D.A. Firsov, and V.M. Bondar, Zh. Eksp. Teor. Fiz. **69**, 638 (1999) [JETP Lett. **69**, 676 (1999)].
[8] E.F. Schubert and K. Ploog, Phys. Rev. B **30**, 7021 (1984).
[9] R.J. Nelson, Appl. Phys. Lett. **31**, 351 (1977).
[10] D.V. Lang and R.A. Logan, Phys. Rev. Lett. **39**, 635 (1977).
[11] U. Fano, Phys. Rev. **124**, 1866 (1961).
[12] P.A.M. Dirac, *Principles of Quantum Mechanics*, 4th ed. (Clarendon Press, Oxford, 1981), p. 314.
[13] L.D. Landau and E.M. Lifshitz, *Quantum Mechanics. Non-relativistic Theory*, 3rd ed., (Pergamon Press, Oxford, 1977).
[14] P.Y. Yu and M. Cardona, *Fundamentals of Semiconductors*, 2nd ed., (Springer-Verlag, Berlin, 1999), p. 160.
[15] J. H. Davies, *The Physics of Low-Dimensional Semiconductors* (Cambridge University Press, Cambridge, 1998), p. 355.
[16] C. Guillemot, M. Baudet, M. Gauneau, and A. Regreny, Phys. Rev. B **35**, 2799 (1987).
[17] U. Penner, H. Rücker, and I.N. Yassievich, Semicond. Sci. Technol. **13**, 709 (1998).